

Scientific Paper

Doi: <http://dx.doi.org/10.1590/1809-4430-Eng.Agric.v43n5e20220196/2023>

DYNAMIC MONITORING OF HARVESTER WORKING PROGRESS BASED ON TRAVELING TRAJECTORY AND HEADER STATUS

Chen Cong^{1,2}, Cao Guangqiao^{1*}, Zhang Jinlong¹, Hu Jianping^{2*}

^{1*}Corresponding author. Nanjing Institute of Agricultural Mechanization, Ministry of Agriculture and Rural Affairs/Nanjing, China.
Email: caoguangqiao@126.com | ORCID ID: <https://orcid.org/0000-0002-9364-3376>

^{2*}Corresponding author. School of Agricultural Engineering, Jiangsu University/Zhenjiang, China.
Email: Hujp@ujs.edu.cn | ORCID ID: <https://orcid.org/0000-0002-4345-2619>

KEYWORDS

cross-region
mechanical
harvesting, working
progress, dynamic
monitoring, satellite
positioning,
harvesting status.

ABSTRACT

China's socialized service industry of agricultural machinery emerged as the times required, which resolved the institutional contradiction between small farm households and large-scale agriculture. However, as cross-operation harvesters are still monitored based on phone calls, the monitoring efficiency and real-time performance are relatively poor. To improve the dynamic monitoring accuracy of harvester working areas, we proposed a working progress monitoring method based on harvester traveling trajectory and header status identification. The position and gap bridge angle information of harvesters was synchronously acquired in real-time. The height of the header above ground was calculated to determine whether the harvester was harvesting on a valid trajectory. Finally, the valid trajectory of the harvester was selected for area calculation. Field experiments showed that the header heights at the working and non-working tracing points collected by the system were discretely distributed at intervals of [0m, 0.5m] and (0.5m, 2m), respectively. The working progress monitoring algorithm proposed in this paper effectively improved the monitoring accuracy of harvester working areas. The mean error between the working areas calculated with identifying the header status and the actual cultivated land area in the five test plots was 0.09 hm², with a mean error rate of 3.10%, 8.59% lower than that without identifying the harvester header status.

INTRODUCTION

In 1978, China began to implement the household contract responsibility system for farmland in rural areas, a game-changer to the collective operation system by distributing farmlands to individual households assuming full responsibility for their profits and losses, which greatly enhanced farmers' production enthusiasm. However, with the fast development of China's economy and the rapid transfer of rural labor to secondary and tertiary industries, the aging and feminization of agricultural labor became increasingly prominent. The question of "who would cultivate the land" needed to be answered. In 2004, the socialized service industry of agricultural machinery emerged as the times required, which resolved the institutional contradiction between small farm household and large-scale agriculture and

properly answered the question of "who would cultivate the land" in China. Currently, the mechanized harvesting of three staple food crops (rice, corn, and wheat) has the largest scale in agricultural machinery socialized services in China. Many organizations of grain machinery harvesting service have grown into regional or even national leading enterprises, with hundreds of agricultural machines and working areas spanning most provinces. Business owners need to dispatch harvesters and monitor and the harvesting route to maximize economic benefits. At present, harvester operations are dynamically monitored and dispatched based on phone calls, with relatively poor efficiency and real-time performance.

In recent years, great progress has been made in GPS, sensor, remote sensing, and electronic information technologies in the agricultural equipment field. Some

¹ Nanjing Institute of Agricultural Mechanization, Ministry of Agriculture and Rural Affairs/Nanjing, China.

² School of Agricultural Engineering, Jiangsu University/Zhenjiang, China.

Area Editor: Renildo Luiz Mion

Received in: 10-27-2022

Accepted in: 10-26-2023

scholars have applied the above technologies in the dynamic monitoring of agricultural machinery working areas. There are two main methods for dynamic monitoring of agricultural machinery working areas: remote sensing (Sishodia et al., 2020) and GPS technology. In the aspect of working area monitoring based on remote sensing, the quantitative retrieval of crop area using leaf area index (LAI) is a research hotspot (Chen et al., 2022; Guo et al., 2023). For example, Koichi et al. (2022) used wide-angle time-lapse photography to monitor the planting area of eggplant. Maselli et al. (2020) combined standard meteorological data with Sentinel-2 (S-2) multichannel spectrometer (MSI) NDVI images to estimate the irrigated farmland area in the Mediterranean. Yang et al. (2019) applied the random forest (RF) classification algorithm to the time images of Landsat-8 Operational Land Imager (OLI) obtained in Heilongjiang Province (1,235 scenes) in 2015 and 2016, and proposed an integrated method for monitoring changes in the planting areas of corn, soybean, and rice. However, limited by the satellite access frequency, the timeliness of satellite remote sensing is significantly reduced. The access period of GF-1 satellite in China is four days (Guo et al., 2021), which cannot meet the scheduling requirement of mechanical harvesting operations.

In working area monitoring by GPS, traditional GPS area measurement is performed by collecting the latitude and longitude of fixed points in the field with a hand-held land area acre meter, which is inefficient (Maciej et al., 2020; Sandeep, 2021). The area of cultivated land is measured by a hand-held acre meter, which requires registration of the measurement trajectory with possible over estimation of the trajectory length (Liu et al., 2019). As a result, the measured area can be larger than the actual one. Song et al. (2020) believed that measurement errors depended on the measurement area and gradually decreased as measurement areas increased. For automatic measurement and monitoring of agricultural machinery working areas, the acquisition of agricultural machinery trajectory using a vehicle-mounted GPS terminal to implement dynamic monitoring of the working progress through the corresponding algorithm has become a research hotspot. Based on cutting width and a constant forward speed of a combine, Wu et al. (2022) determined harvest area using a microwave ranging system (Rukan & Dilek, 2022). Zhang et al. (2022) designed a radar speed measurement system based on CAN bus and microwave Doppler radar sensor, so the measured speed of tractor and working width can be used to calculate the work area. Zhang et al. (2020) determined harvest areas by Beidou in a real-time kinematic mode. Zhang et al. (2018) developed

a GPS system to monitor agricultural machinery working areas based on the Android system, which implemented monitoring, statistics, and management of agricultural machinery working area and trajectory. Bai et al. (2022) designed a vehicle-mounted farmland area measurement system with a relative error of 4%. Lu et al. (2015) selected double satellite positioning (GPS and Galileo satellites) receivers to collect positioning data and calculate the tractor working area, with a relative error of 2.09% in the test plot. Li et al. (2023) used Beidou positioning terminal to collect real-time track information for agricultural machinery and calculated the effective working area of the machinery through analysis with a spatial clustering algorithm, resulting in a statistical error of less than 2% for the effective working area. However, the above GPS monitoring methods ignored non-working trajectories such as agricultural machinery turning around and field transfer. Good test results were obtained under test conditions with regular plots and large areas. However, in the actual production of finely divided plots, agricultural machinery has to turn around frequently, and the accuracy of such methods is questionable.

Given the above issues, this paper proposed a method for monitoring the working progress based on harvester traveling trajectory and header status identification. The position and gap bridge angle information of the harvester was acquired in real-time synchronously. The height of the header above ground was calculated to determine whether the harvester was in the harvesting state on a valid trajectory. Finally, the valid trajectory of the harvester was selected for the area calculation to improve the measurement accuracy of the working area and provide a solution for remote dynamic monitoring of the agricultural machinery working progress on the finely-divided cultivated land in southern China.

Data Acquisition and Communication System

In this paper, an angular transducer, Beidou positioning module, GPRS communication module, and CPU module were selected to form a harvester data acquisition terminal. The specific system framework is shown in Figure 1. The system is powered by a 12V DC power supply from the on-board battery of the harvester. The angular transducer is installed on the harvester gap bridge to collect the gap bridge angle of the harvester in real-time. The Beidou positioning module receives Beidou satellite positioning data on the latitude and longitude of the harvester in real-time. The gap bridge angle and latitude/longitude data of the harvester are transmitted back to the server through the GPRS module at a frequency of 12 times/min.

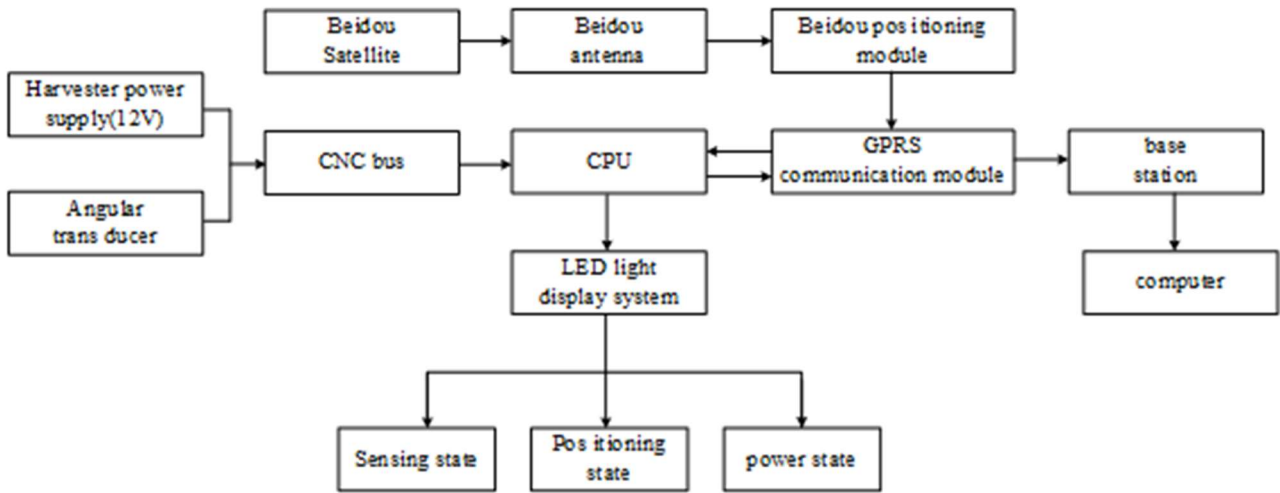


FIGURE 1. Framework diagram of harvester working data acquisition system.

Calculation method of header height

In this paper, the angle α between the harvester gap bridge surface and the ground plane was collected by an angular transducer. Combined with the fixed height (H) from the harvester gap bridge shaft to the ground and the bridge length L (see Figure 2.), the height (h) from the header cutter of the harvester to the bottom of the carriage wheel is calculated based on [eq. (1)].

$$h = H - L \sin \alpha \tag{1}$$

Due to the heavyweight of the harvester, its wheels will sink when traveling in the unhardened farmland. Hence, the wheel settlement depth η should be introduced to calculate the height h^* of the header above ground based on [eq. (2)]. The value of η is determined by factors such as the weight of the harvester, the tire contact area, and the depth of soil mud feet. As various harvesting models and soil conditions have different values of η , the value of η in the target area should be tested before the work area is monitored.

$$h^* = h - \eta \tag{2}$$

The h^* is used to determine whether the harvester is working. If so, the height of the header will be lowered to adapt to that of the crop ear. In general, when a rice and wheat combine harvester is working, the height of the header above ground should not exceed the lowest crop ear height (A). When the harvester is turning around or traveling on the road, the height of the header will be raised to protect the cutter safety and avoid damage due to collision with crop ears. At this time, the height of the header above ground will be higher than A . Hence, the effective trajectory of the harvester can be identified by [eq. (3)].

$$\begin{cases} h^* \leq A, & \theta = 1 \\ h^* > A, & \theta = 0 \end{cases} \tag{3}$$

Where θ is the discrimination coefficient of the harvester trajectory. When $\theta = 1$, the harvester is working, and the movement trajectory is valid; when $\theta = 0$, the harvester is not working, and the movement trajectory is invalid.

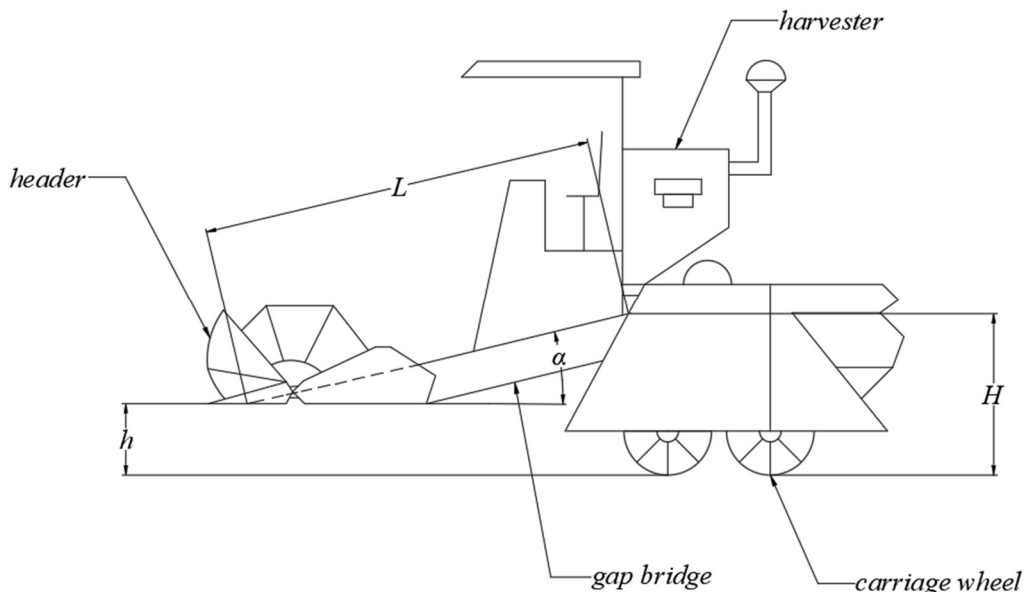


FIGURE 2. Harvester body parameters.

Calculation method of the working area

Gaussian projection algorithm

As the Beidou positioning system adopts CGCS2000 ellipsoid coordinates (B, L), for the convenience of area calculation, the ellipsoid coordinates should be projected to the rectangular plane coordinates (X, Y). Gaussian projection is the most commonly used projection method, also known as the equal-angle transversal elliptic cylindrical projection. Upon projection, it is assumed that an elliptical cylinder is transverse to a meridian of the earth ellipsoid, namely the central meridian. Based on the equiangular condition, the points on the ellipsoid surface of the earth are projected onto the elliptical cylinder using the mathematical analysis method and expanded into a plane along the generatrix of the elliptical cylinder. Subsequently, a rectangular coordinate system can be established on this plane: With the intersection of the central meridian and the equatorial projection as the origin, the central meridian projection as the X-axis, the positive direction points to the north geographic pole, the equatorial projection as the Y-axis, and the direction toward the east is positive. The projection formula from a point (B, L) on the ellipsoid to a point (x, y) in the Gauss plane rectangular coordinate system is shown in [eq. (4)] and [eq. (5)] (Feng et al., 2020).

$$x = f(B, l) = S + \frac{1}{2} Nt \cos^2 Bl^2 + \frac{1}{24} Nt(5 - t^2 + 9\eta^2 + 4\eta^4) \cos^4 Bl^4 + \frac{1}{720} Nt(61 + 58t^2 - t^4 + 270\eta^2 - 330t^2\eta^2) \cos^6 Bl^6 + \dots \tag{4}$$

$$y = g(B, l) = N \cos Bl + \frac{1}{6} N(1 - t^2 + \eta^2) \cos^3 Bl^3 + \frac{1}{120} N(5 - 18t^2 + t^4 + 14\eta^2 - 58t^2\eta^2) \cos^5 Bl^5 + \dots \tag{5}$$

Where:

- $l = L - L_0$, L_0 is the central meridian;
- e and e' are the first and second eccentricity of the reference ellipsoid respectively;
- $\eta = e' \cos B$,
- $t = \tan B$,
- N is the curvature radius of the normal section, and

S is the meridian arc length from the equator to the latitude B , which can be calculated based on the following equation.

$$S = a_0 B - \frac{a_2}{2} \sin 2B + \frac{a_4}{4} \sin 4B - \frac{a_6}{6} \sin 6B + \frac{a_8}{8} \sin 8B \tag{6}$$

$$\begin{cases} a_0 = m_0 + \frac{1}{2} m_2 + \frac{3}{8} m_4 + \frac{5}{16} m_6 + \frac{35}{128} m_8 \\ a_2 = \frac{1}{2} m_2 + \frac{1}{2} m_4 + \frac{15}{32} m_6 + \frac{7}{16} m_8 \\ a_4 = \frac{1}{2} m_4 + \frac{3}{16} m_6 + \frac{7}{32} m_8 \\ a_6 = \frac{1}{32} m_6 + \frac{1}{16} m_8 \\ a_8 = \frac{1}{128} m_8 \end{cases} \tag{7}$$

$$\begin{cases} m_0 = a(1 - e^2) \\ m_2 = \frac{3}{2} e^2 m_0 \\ m_4 = \frac{5}{4} e^2 m_2 \\ m_6 = \frac{7}{6} e^2 m_4 \\ m_8 = \frac{9}{8} e^2 m_6 \end{cases} \tag{8}$$

Working area algorithm

Assuming that the agricultural machinery working trajectory contains $n+1$ spatial operation tracing points, namely P_1, P_2, \dots, P_{n+1} , the tracing points are connected in chronological order to generate primitive line segments L_1, L_2, \dots, L_n . The primitive line segment set L of agricultural machinery working spatial operation trajectory is:

$$L = \bigcup_{i=1}^n L_i \tag{9}$$

The primitive line segments in the set L are all travel trajectory line segments, including working travel trajectory line segments and non-working travel trajectory line segments such as U-turns and turns. Through the height of the header at the tracing point P_i , the working status of the primitive line segment L_i is determined; that is, the validity of L_i is determined based on the value of θ_i , as shown in Figure 3.

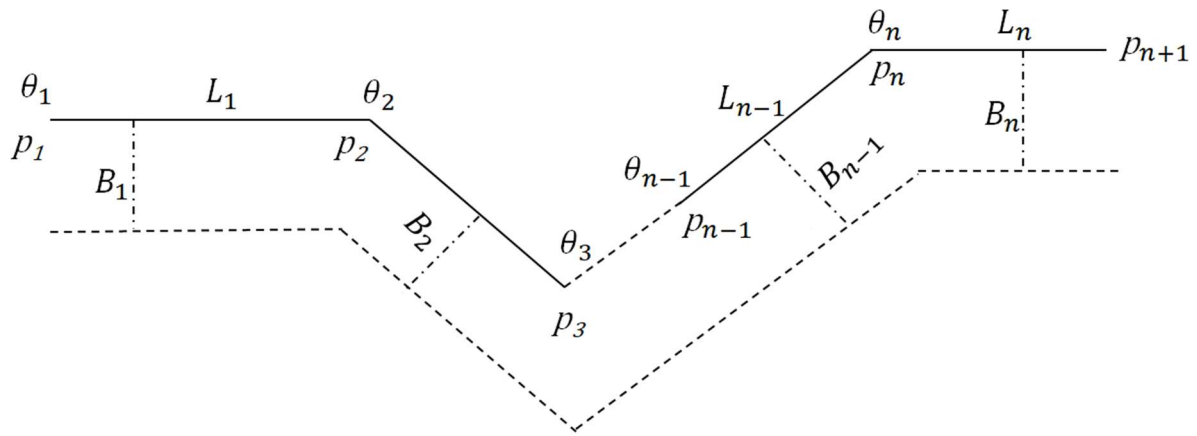


FIGURE 3. Schematic diagram of harvester working area algorithm.

Note: $p_1, p_2, p_3, \dots, p_{n-1}, p_n, p_{n+1}$ are the tracing point of the harvester operation; $L_1, L_2, \dots, L_{n-1}, L_n$ are the primitive line segments of the trajectory of the harvester; $\theta_1, \theta_2, \theta_3, \dots, \theta_{n-1}, \theta_n$ are the discriminant coefficient of primitive line segment; $B_1, B_2, \dots, B_{n-1}, B_n$ is the harvesting width.

The working area of the harvester is composed of the primitive line segment set of effective operations and working widths of the harvester. When the harvester travels to the $i=n+1$ tracing point, the working area (S_n) is calculated as follows:

$$S_n = \sum_{i=2}^{n+1} B_i \theta_i \sqrt{(x_i - x_{i-1})^2 + (y_i - y_{i-1})^2} \quad (10)$$

Area Algorithm Verification

Test equipment and conditions

In October 2021, a dynamic monitoring experiment on the mechanized rice harvesting area was conducted at the Huanghai Farm in Xiangshui County, Jiangsu, China. The John Deere C230 grain combine harvester was used as the test

platform. The working width of this harvester was 4.57 m, the height H of the shaft connecting the bridge and the vehicle body was 1.7m, and the length L from the shaft to the bottom of the header was 4.5m. The self-developed data acquisition system was installed on the experimental combine harvester. The angular transducer was attached to the upper surface of the harvester gap bridge, and the Beidou positioning module was affixed to the front middle of the harvester granary top surface. In the experiment, 5 cultivated land plots with an area of about 3 hectares, same rice varieties, consistent growth, an average height (A)50cm of the lowest ear of rice, and equivalent soil moisture. The grain truck follows the harvester to receive the grain, and the load of the harvester has little changes. The test shows that the wheel settlement depth η is 0.1m. In the experiment, the harvester kept full-width harvesting.



FIGURE 4. John Deere C230 grain combine harvester used in the test.

RESULTS AND DISCUSSION

Working trajectory of harvester

Harvester drivers with 25 years of experience at the Huanghai Farm Agricultural Machinery Station were responsible for driving the harvester for harvesting at T1, T2,

T3, T4, and T5, independently. The data acquisition system transmitted the latitude, longitude, and gap bridge angle data of the harvester position to the server in real-time at an acquisition frequency of once every 5s). Subsequently, the working trajectory of the harvester was plotted based on ArcGIS, as shown in Figure 5.

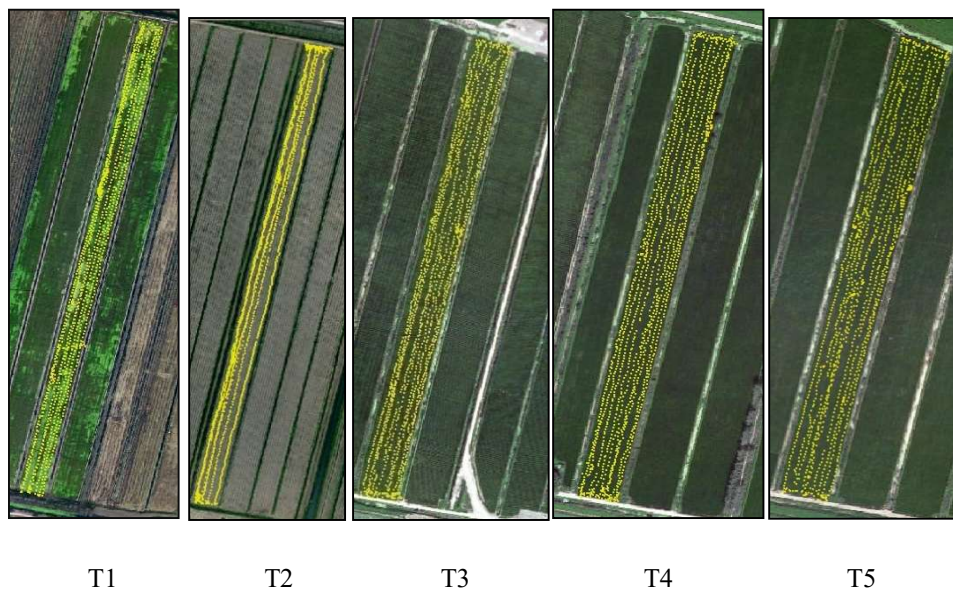


FIGURE 5. Working trajectory of harvester.

Figure 5 shows that all test plots are long strips, and the terrain conditions have little impact on the efficiency of the harvester. The plots are inconsistent in the aspect ratio, especially the plot widths, which are significantly different.

The harvester works according to the route of harvesting along the long side and turning around on the short one. Hence, more tracing points are clustered at the shorter boundary of the plot.

TABLE 1. General situation of tracing points in the test plots.

Plot number	Number of tracing points	Longitude distribution	Latitude distribution	Total trajectory length (m)
T1	1927	(E119.984983°, E119.987320°)	(N34.259099°, N34.266982°)	7724.30
T2	1997	(E119.961129°, E119.963502°)	(N34.300177°, N34.308231°)	8140.04
T3	1881	(E119.955955°, E119.957694°)	(N34.319387°, N34.324651°)	5858.80
T4	1804	(E119.959675°, E119.961310°)	(N34.318710°, N34.323552°)	5955.04
T5	1655	(E119.969227°, E119.970816°)	(N34.317037°, N34.321504°)	5446.86

Table 1 shows that the 5 test plots have significantly different numbers of tracing points, with a maximum of 1,997 points in plot T2 plot and a minimum of 1,655 points in plot T5. The lengths of field traveling trajectories are also significantly different, with a maximum of 8,140.04 m in plot T2 and a minimum of 5,446.86 m in plot T5. There is no linear relationship between the number of tracing points and the length, suggesting that the traveling speed of the harvester is

not entirely consistent during the operation.

Header height of harvester above ground

The gap bridge angle of the harvester corresponding to each tracing point is calculated according to [eq. (1)] and [eq. (2)] to obtain the heights of the header above ground. The heights of the header above ground replotted in chronological order, as shown in Figure 6.

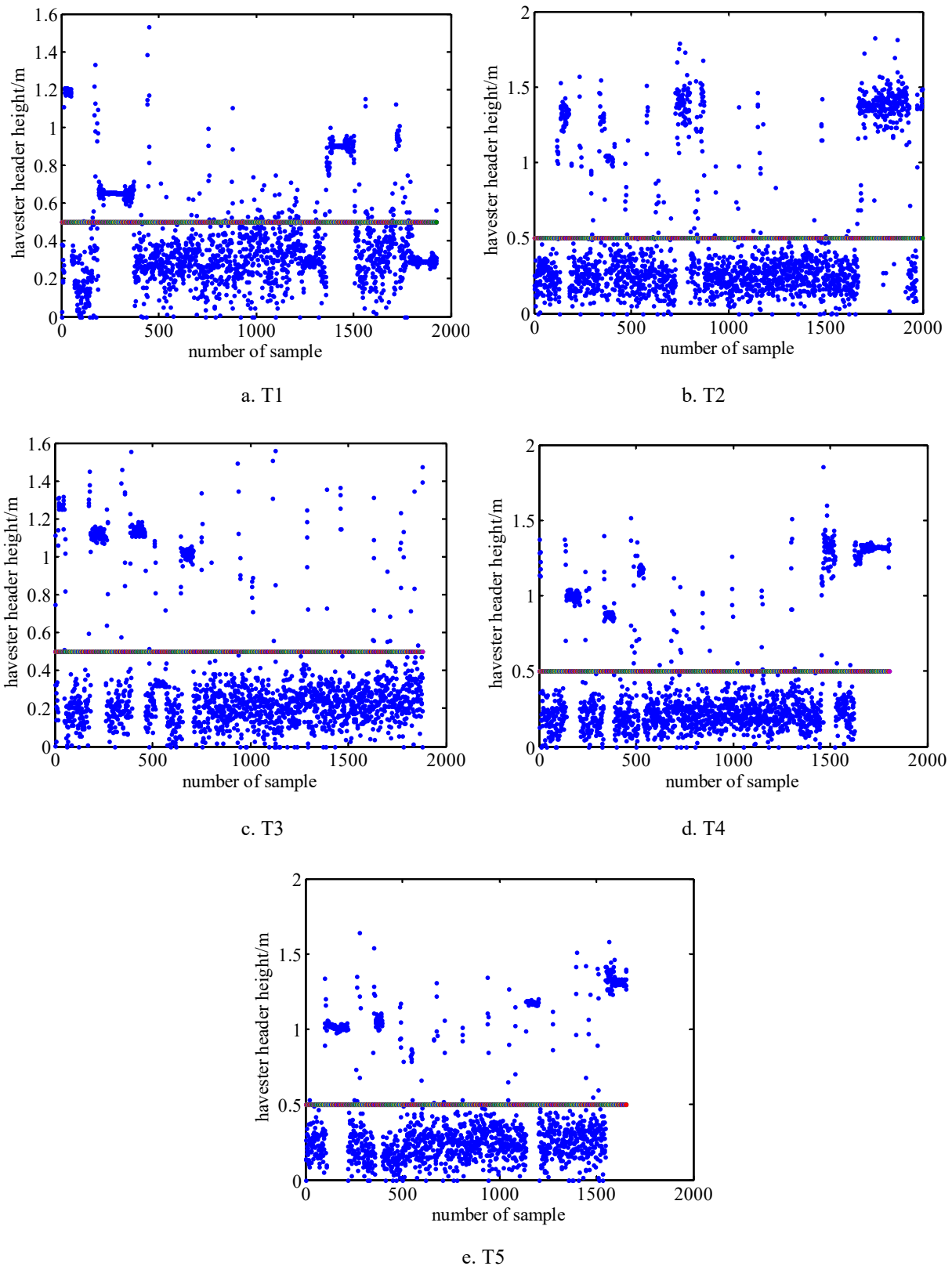


FIGURE 6. Header height of the harvester at different points.

It is not difficult to see that the header height data of the harvester are relatively discrete, and the height values fluctuate in the interval $[0m, 2m]$. However, the height values at most points are below 0.5 m. According to [eq.(3)], the points where the head height is in the interval $[0m, 0.5m]$ are working tracing points, and those in the interval $(0.5m, 2m)$ are non-working ones. The two types of tracing points can be clearly distinguished by the horizontal marking line in Figure 7. The header heights at the working tracing points are

discretely distributed in the interval $[0m, 0.5m]$, and the points with height values in the interval $[0.2m, 0.4m]$ are relatively concentrated (see Figure 7 for details); the non-working tracing points are longitudinally distributed discretely in the interval $(0.5m, 2m)$ and horizontally distributed at a certain interval, which conforms to the harvester movement pattern of making a U-turn after completing a certain working range. However, there are also many outliers in the non-working trajectory. Figure 8b shows

that the header height values at many tracing points are concentrated at around 1.2m–1.4m. Because the soil moisture of the test plot selected in this paper is balanced, there will be no sudden change in wheel settlement; that is, the value of η is basically unchanged, and the fixed

parameters H and L of the harvester are constant. It can be seen that the angle α continues to decrease; that is, the driver lifts the header for a long time, mainly in the following situations: machine failure troubleshooting, driver resting, or waiting for the grain truck.

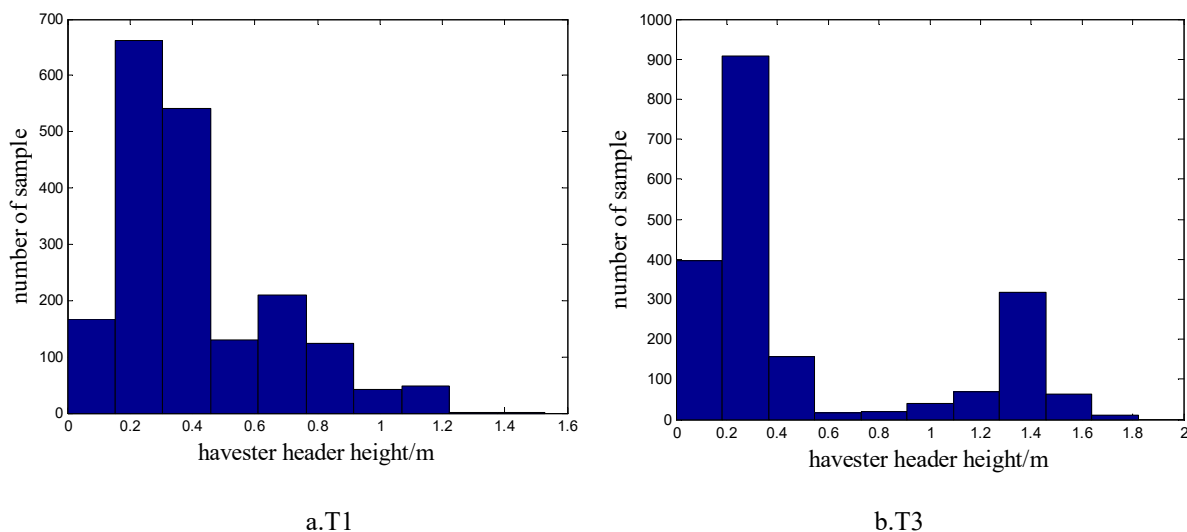


FIGURE 7. Histogram of the header height distribution.

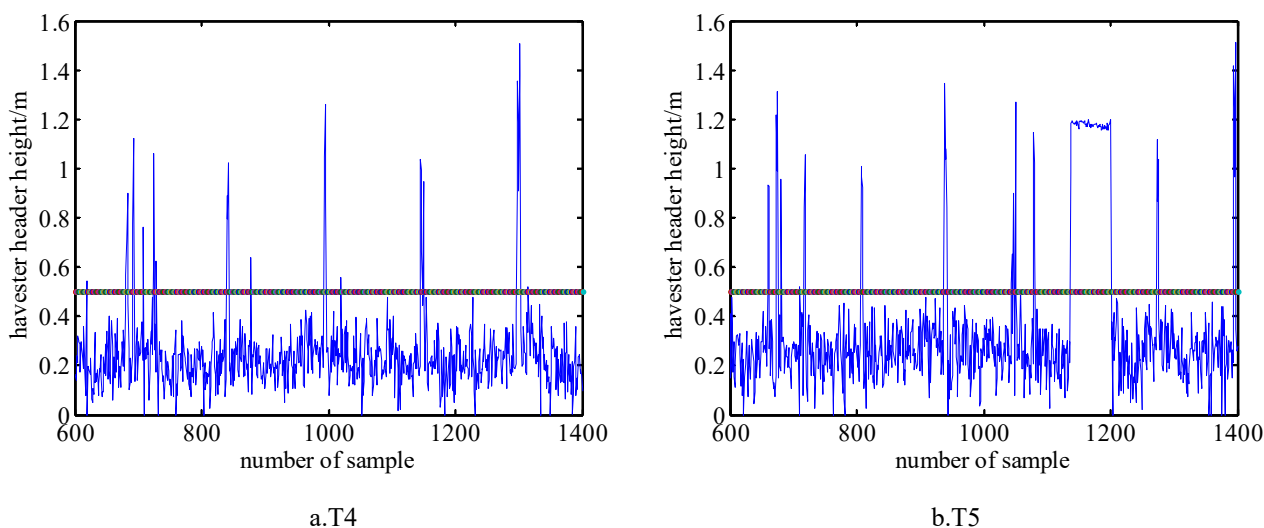


FIGURE 8. Header height of the harvester at the 600–1400th tracing points.

The 600–1400th tracing point data of plots T4 and T5 were intercepted to plot Figure 8. The figure clearly shows that the non-working tracing points are regularly clustered. It can be understood that as lifting and lowering the header when the harvester is turning, the cluster interval is about 100–200 points depending on different lengths of continuous operation, that is, a straight-line operation is

completed every 8–16 min.

Working area results

According to [eq. (10)], the working areas of the harvester in 5 test plots were calculated, respectively. The actual areas of test plots and the working areas without identifying the header were compared to obtain Table 2.

TABLE 2. Comparison of working area calculation results.

Plot number	Actual area of cultivated land (hm ²)	Working area without identifying the header (hm ²)	Working area with identifying the header (hm ²)
T1	3.26	3.53	3.41
T2	3.12	3.72	3.24
T3	2.54	2.68	2.62
T4	2.35	2.72	2.40
T5	2.27	2.49	2.31

Table 2 shows that the harvester working progress monitoring algorithm based on the working trajectory and header status designed in this paper can reduce the monitoring accuracy of the harvester working area. The mean error between the working area and the actual area of the cultivated land calculated by identifying the header status in the five test plots is 0.09 hm², and the mean error rate is 3.10%; whereas the mean error of the working area calculated without identifying the header status (the product of harvester trajectory length and cutting width) is 0.32 hm², and the mean error rate is 11.69%. The working areas calculated by the two methods are larger than the actual areas of the cultivated land. In general, the working area calculated without identifying the header status > that calculated with identifying the header status > the actual area of the cultivated land.

Discussion

Header height data stability

In this paper, the gap bridge angle of the harvester was collected by an angular transducer in real-time and converted to obtain the dynamic height data of the harvester header. Figures 7 and 8 show that the header height data of the harvester are unstable with significant fluctuation. Even during the stable working stage of the harvester, the header height still fluctuates significantly. In general, during the harvesting operation of the harvester, the header will remain stable to ensure the consistent cutting height and stable harvest quality. Data fluctuations may be caused by the following reasons. Firstly, large vibrations are produced by the engine, gearbox, traveling system, threshing system, transmission system, etc., during the working process of the harvester, especially the threshing system. The stability of the sensor is affected by machine vibration, as shown in Figure 8.b. The height of the header between the 1150–1200th points is consistent and stable at about 1.2 m, with minimal fluctuation. The latitude and longitude data of the points in this interval basically remain unchanged and stable at (N34.31902°, E119.96989°). That is, the harvester is in a static state at this stage without any vibration. Hence, data can be collected by the sensor stably. Secondly, the flatness of the paddy field is relatively poor, and the machine body moves up and down with the terrain during the traveling process, which affects the stability of header height data.

Calculation error of working area

The working progress monitoring algorithm proposed in this paper was used to calculate the working area, and the average accuracy obtained through field experiments was 96.9%, equivalent to the 96%–97% accuracy obtained by Lu et al. (2015) using the working trajectory to monitor the

tractor cultivated land area. There are two main rules in the errors of the algorithm proposed in this paper. Firstly, all the monitoring working areas were larger than the actual areas of cultivated land. The reason was that in the harvester working process, to avoid missed harvesting, it was impossible to implement full-width harvesting throughout the whole process. Partially adjustable redundant cutting width was generally set aside. However, the harvester was set to full-width harvesting in this experiment, without real-time monitoring of its working width. Therefore, the test result is larger. Secondly, the larger the test plot area, the higher the error rate. Table 2 shows that as the test plot area increases, the error rate of the algorithm proposed in this paper increases from 1.76% to 4.60% successively. The reason is that the working calculation error mainly occurs in the transition stage of harvesting–turning–harvesting. For example, at the end of a harvesting strip, the header of the harvester will not be raised immediately due to the lag in operation. Before entering a new harvesting strip, the header will also be lowered in advance. Therefore, when the length of the cultivated land is fixed, the larger the cultivated area is, the more times the harvester turns, the higher the error is.

improvement plan for data collection system

The monitoring of homework progress in this article relies on the trajectory point data and header data collected by the designed data collection system. The quality of these data has a significant impact on the monitoring results. The system in this article has two problems. Firstly, the frequency of data collection can be further improved. At present, the data collection frequency is once every 5 seconds. When the harvester travels at a high speed, a 5-second time interval can cause information deviation, which affects the accuracy of monitoring results. Secondly, the harvester's cutting range is not monitored synchronously. When the field is small, there may be a certain area that cannot be fully harvested, resulting in a larger monitoring result. Therefore, in the future, the collection frequency of the data collection system will be increased to monitor 1 data every 2 seconds, and the actual cutting width value of the harvester will be synchronously collected using image sensors, further improving the monitoring accuracy of the method proposed in this article.

CONCLUSIONS

(1) To improve the dynamic monitoring accuracy of the harvester working progress, a working progress monitoring method based on the harvester traveling trajectory and header status identification was proposed. The position and gap bridge angle information of the harvester was

acquired in real-time synchronously to calculate the height of the header above ground and determine whether the harvester was harvesting on a valid trajectory. Finally, the valid trajectory of the harvester was selected for the area calculation. This method improved the calculation error rate by 8.59% compared with that without identifying the header status.

(2) Field experiments showed that the header height data of the harvester were relatively discrete, and the height values fluctuated in the interval [0m, 2m]; the header heights at the working tracing points were discretely distributed in the interval [0m, 0.5m], and the height values were relatively concentrated in the interval [0.2m, 0.4m]. The non-working tracing points were distributed longitudinally in the interval (0.5m, 2m), and horizontally at a certain interval. The fluctuation of header data was mainly affected by machine vibration and field flatness.

(3) The harvester working progress monitoring algorithm based on the working trajectory and header status designed in this paper could improve the monitoring accuracy of the harvester working area. The mean error between the working area and the actual area of the cultivated land calculated by identifying the header status in the five test plots was 0.09 hm², and the mean error rate was 3.10%. Moreover, all the monitoring working areas were larger than the actual areas of the cultivated land. The larger the test plot area, the higher the error rate.

(4) The test device designed in this paper cannot monitor the dynamic changes in the working width of the harvester in real-time. Although the driver tries to control the harvester and keep full-width harvesting, the deviation cannot be avoided entirely, causing a larger test result. In the follow-up research, we will improve the test device and method, automatically monitor the working width of the harvester through machine vision, and further improve the dynamic monitoring accuracy of its working area.

FUNDING

This work was supported by a grant of the special funding for basic scientific research business expenses of central public welfare scientific research institutes (S202215); Science and Technology Innovation Project of Chinese Academy of Agricultural Sciences (Academy of Agricultural Sciences Office (2014) No.216).

ACKNOWLEDGMENTS

The authors would like to thank the anonymous reviewers and the editor for their constructive comments and suggestions for this study.

REFERENCES

- Bai J, Liu B, Liu P, Li H (2022) Design of information collection system for subsoiling operation. *Journal of North University of China (Natural Science Edition)* 43(3): 267-272+280. <https://doi.org/10.3969/j.issn.1673-3193.2022.03.011>
- Chen ZL, Jia K, Wei XQ, Liu Y, Zhan YL, Xia M, Yao YJ, Zhang XT (2022) Improving leaf area index estimation accuracy of wheat by involving leaf chlorophyll content information. *Computers and Electronics in Agriculture* 196(5): 106902. <https://doi.org/10.1016/j.compag.2022.106902>
- Feng LG, Jin LX, Bian SF, Li HP (2020) Application of large ellipsoid parameter model in long linear engineering. *Geomatics and Information Science of Wuhan University* 45(2): 219-225+232. <https://doi.org/10.13203/j.whugis20180133>
- Guo AT, Ye HC, Huang WJ, Qian BX, Wang JJ, Lan YB, Wang SZ (2023) Inversion of maize leaf area index from UAV hyperspectral and multispectral imagery. *Computers and Electronics in Agriculture* 212: 108020. <https://doi.org/10.1016/j.compag.2023.108020>
- Guo L, Liu Y, He HG, Lin H, Qiu GX, Yang WJ (2021) Consistency analysis of GF-1 and GF-6 satellite wide field view multi-spectral band reflectance. *Optik* 231(4): 166414. <https://doi.org/10.1016/j.ijleo.2021.166414>
- Koichi N, Masahiko S, Mizuho K, Yudai G, Koyo N, Hiromi Y, Tadashige I, Tomihiro Y, Ikunao T, Masaharu K (2022) Leaf area index estimation of a row-planted eggplant canopy using wide-angle time-lapse photography divided according to view-zenith-angle contours. *Agricultural and Forest Meteorology* 319(5): 108930. <https://doi.org/10.1016/j.agrformet.2022.108930>
- Li XH, Bai JQ, Wu XZ, Hao FQ (2023) Statistical on agricultural machinery operation area based on Beidou positioning data. *IEEE 3rd Information Conference on Information Technology, Big Data and Artificial Intelligence (ICIBA 2023)*. <https://doi.org/10.1109/ICIBA56860.2023.10165601>
- Liu JH, Wang JH, Chen MY. (2019) Estimating the trajectory length of buoyant turbulent jet flames issuing from a downward sloping nozzle. *Process Safety and Environmental Protection* 132(12): 153-159. <https://doi.org/10.1016/j.psep.2019.09.030>
- Lu ZX, Zhong WJ, Diao XY, Mei SK, Zhou J, Cheng Z (2015) Measurement of field area based on tractor operation trajectory. *Transactions of the Chinese Society of Agricultural Engineering* 31(19): 169-176. <https://doi.org/10.11975/j.issn.1002-6819.2015.19.023>
- Maciej MN, Katarzyna D, Lukasz L, Julian C (2020) Mobile GIS applications for environmental field surveys: a state of the art. *Global Ecology and Conservation* 23: e01089. <https://doi.org/10.1016/j.gecco.2020.e01089>
- Maselli F, Battista P, Chiesi M, Rapi B, Angeli L, Fibbi L, Magno R, Gozzini B (2020) Use of Sentinel-2 MSI data to monitor crop irrigation in Mediterranean areas. *International Journal of Applied Earth Observation and Geoinformation* 93(12): 102216. <https://doi.org/10.1016/j.jag.2020.102216>
- Rukan CS, Dilek V (2022) Performance of microwave reactor system in decomposition of ammonia using nickel based catalysts with different supports. *International Journal of Hydrogen Energy* 47(34): 15175-15188. <https://doi.org/10.1016/j.ijhydene.2020.109118>

Sandeep K (2021) GPS based handheld system for land area measurement. *International Journal for Research in Applied Science and Engineering Technology* 9: 1619-1624. <https://doi.org/10.22214/IJRASET.2021.35302>

Sishodia RP, Ray RL, Singh SK (2020) Applications of remote sensing in precision agriculture: a Review. *Remote Sensing* 12(19): 3136. <https://doi.org/10.3390/rs12193136>

Song C, Liu L, Feng G, Fan Y, Xu SY (2020) Coverage control for heterogeneous mobile sensor networks with bounded position measurement errors. *Automatica* 120(10): 109118. <https://doi.org/10.1016/j.automatica.2020.109118>

Wu CC, Chen Y, Yang WZ, Yang LL, Qiao P, Ma Q, Zhai WX, Li D, Zhang XQ, Wan CF, Li GY, Huang JH, Tian WZ, Fan XF, Tan LJ, Su CH (2022) Construction of big data system of agricultural machinery based on BeiDou. *Transactions of the Chinese Society of Agricultural Engineering (Transactions of the CSAE)* 38(5): 1-8. <https://doi.org/10.11975/j.issn.1002-6819.2022.05.001>

Yang LB, Wang LM, Huang JF, Lamin RM, Ruzemaimaiti M (2019) Monitoring policy-driven crop area adjustments in northeast China using Landsat-8 imagery. *International Journal of Applied Earth Observation and Geoinformation* 82(10): 101892. <https://doi.org/10.1016/j.jag.2019.06.002>

Zhang DH, Ma YH, Guan F, Wang Q, Zheng T (2018) Agricultural machinery operation area and track monitoring management system based on GPS. *Geospatial Information* 16 (02): 68-70+11. <https://doi.org/10.3969/j.issn.1672-4623.2018.02.023>

Zhang J, Wang X, Wang XZ (2022) Research on velocity measurement system of microwave doppler radar based on CAN Bus. *Journal of Agricultural Mechanization Research* 44(12): 119-123. <https://doi.org/10.13427/j.cnki.njvi.2022.12.034>

Zhang L, Wu BT, Xie JX, Zhang HD, Huang JQ, Li M (2020) Design and test on agricultural machinery operation area management system of Beidou navigation. *Journal of Chinese Agricultural Mechanization* 41(12): 139-146. <https://doi.org/10.13733/j.jcam.issn.2095-5553.2020.12.023>